ISSN 0030-400X, Optics and Spectroscopy, 2012, Vol. 113, No. 6, pp. 596–606. © Pleiades Publishing, Ltd., 2012.

SPECTROSCOPY OF ATOMS AND MOLECULES

Theoretical Investigations on the Molecular Structure and Vibrational Spectral Analysis of 4-Methyl 2-phenylimidazole[1]

Y. Erdogdu, B. Eskioğlu, and M. T. Güllüoğlu

Department of Physics, Ahi Evran Univ. Kirsehir 40040, Turkey

Received March 29, 2012

Abstract—The FT-IR, FT-Raman and FT-NMR spectra of 4-Methyl-2-phenylimidazole (4M2PI)molecule was recorded and analyzed. The tautomeric, structural and spectroscopic analysis of the title molecule was made by using density functional harmonic calculations. For the title molecule, only one tautomeric form was found most stable structure by using B3LYP level with the 6-311G++(d,p) as basis set. Selected experimental bands were assigned and characterized based on the scaled theoretical wave numbers by their total energy distribution (TED).

DOI: 10.1134/S0030400X12090032

INTRODUCTION

The development of new methods for the synthesis of azaheterocycles is of particular interest in organic chemistry since they occur in a wide variety of natural products. This is especially true for nitrogen-containing five-membered ring, such as imidazoles, which are core components of a large number of substances that possess a wide range of interesting biological activities [1–4].

Imidazole is a heterocyclic compound of five-membered diunsaturated ring structure composed of three carbon atoms and two nitrogen atoms at nonadjacent positions. The simplest member of the imidazole family is imidazole itself, colorless to pale yellow crystalline solid with a weak amine like odor; soluble in water and alcohol, melts at 89°C, boils at 256°C. Imidazoles are poorly soluble in water generally, but are dissolved in organic solvents, such as chloroform, propylene, glycol, and polyethoxylated castor oil. Imidazole ring is found in histidine (an essential amino acid) and histamine, the decarboxylated compound from histamine. Imidazole has two nitrogen atoms. The one is slightly acidic, while the other is basic. Imidazole and its derivatives are widely used as intermediates in synthesis of organic target compounds including pharmaceuticals, agrochemicals, dyes, photographic chemicals, corrosion inhibitors, epoxy curing agents, adhesives and plastic modifiers [5]. Some imidazole compounds inhibit the biosynthesis of ergo sterol, required in cell membrane in fungal. They have antibacterial, antifungal, antiprotozoal, and anthelmintic activity. Imidazole and its derivatives are widely used as intermediates in synthesis of organic target compounds including pharmaceuticals, agrochemicals, dyes, photographic chemicals, corrosion inhibitors, epoxy curing agents, adhesives and plastic modifiers [5]. The phenyl imidazole molecular fragment plays a primary role in the functional architecture of biologically active molecules such as novel histamine H2 receptor antagonists [6], cardio tropic agents [7] and several types of artificial enzymes [8–11]. Several distinct phenylimidazoles are therapeutically useful antifungal agents against either superficial or systemic infections FT-IR, FT-Raman and FT-NMR spectra of 4-phenylimidazole molecule using theoretical and experimental methods has been reported earlier [12]. In the present paper, we report the results of theoretical and experimental (FT-IR and FT-Raman and NMR) spectra, conformational analysis and molecular orbital energies of 4M2PI molecule. The spectroscopic properties of 4M2PI have not yet been studied in detail to the best of our knowledge. Therefore, the present investigation was undertaken to study the vibrational spectra of 4M2PI molecule completely and to identify the various normal modes with greater wavenumber accuracy. Density Functional Theory (DFT/B3LYP) calculations have been performed to support our wavenumber assignments. Furthermore, we interpreted the calculated spectra in terms of total energy distributions (TED's) and made the assignment of the experimental bands.

EXPERIMENTAL

The FT-IR spectrum of the title molecule is recorded in the region 4000–400 cm^{-1} on IFS 66V spectrophotometer using KBr pellet technique and is shown in Fig. 1. The FT-Raman spectrum of 4M2PI has been recorded using 1064 nm line of Nd:YAG laser as excitation wavelength in the region 50–3500 cm^{-1} on a Thermo Election Corporation model Nexus 670 spectrophotometer equipped with FT-Raman module

[1] The article is published in the original.

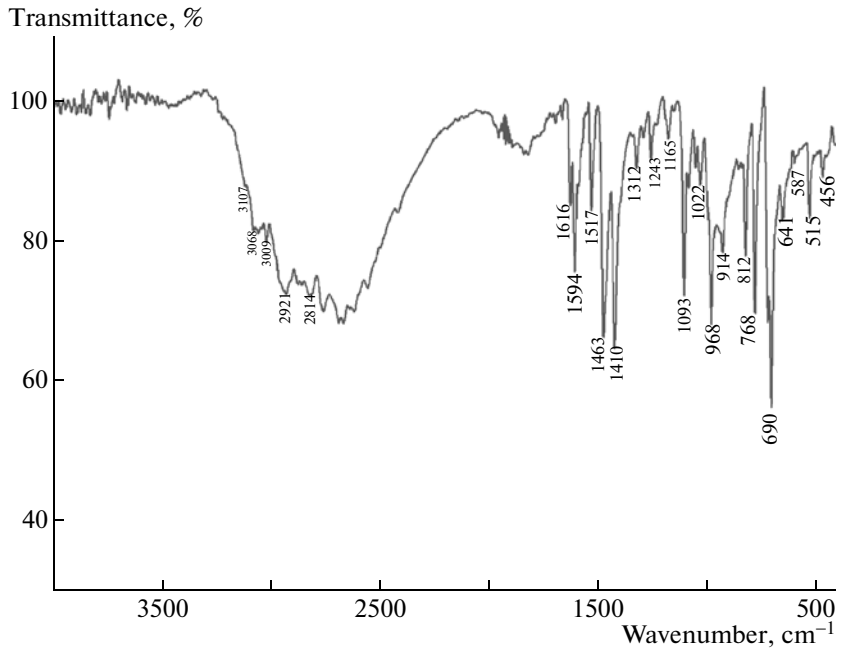

Fig. 1. Experimental FT-IR spectra of 4-methyl-2-phenylimidazole molecule.

accessory and are shown in Fig. 2. The ^{1}H an ^{13}C NMR spectra are taken in chloroform solutions and all signals are referenced to TMS on a BRUKER DPX-400 FT-NMR Spectrometer. All NMR spectra are measured at room temperature.

COMPUTATIONAL DETAILS

Gaussian 09 quantum chemical software was used in all calculations [13]. The optimized structural parameters and vibrational wavenumbers for the 4M2PI molecule were calculated by using B3LYP functional with 6-311G++(d,p) as basis set. The vibrational modes were assigned on the basis of TED analysis using SQM program [14]. Normal coordinate analysis of the title molecule has been earned out to obtain a more complete description of the molecular motions involved in the fundamentals. The calculated harmonic vibrational wavenumbers were scaled down uniformly by a factor of 0.967 (for wave numbers under 1800 cm^{-1}) and 0.955 (for those over 1800 cm^{-1}) for B3LYP/6-311++G(d,p) level of theory, which accounts for systematic errors caused by basis set incompleteness, neglect of electron correlation and vibrational anharmonicity [l5–17].

The ^{1}H and ^{13}C NMR chemical shifts calculations of the most stable form 6f 4M2PI molecule were made by using B3LYP functional with 6-31lG++(d,p) basis set. The GIAO (Gauge Including Atomic Orbital) method is one of the most common approaches for calculating isotropic nuclear magnetic shielding tensors [18, 19]. For the same basis set size GIAO method is often more accurate than those calculated with other approaches [20, 21]. The NMR spectra calculations were performed by Gaussian 09 program package. The calculations reported were performed in chloroform solution using IEF-PCM model as well as gas phase in agreement with experimental chemical shifts obtained in chloroform solution.

Predictions of Raman Intensities

It should be noted that Gaussian 09 package able to calculate the Raman activity. The Raman activities were transformed into Raman intensities using Raint program [22] by the expression:

$$I_i = 10^{-12} \times (\nu_0 - \nu_i)^4 \frac{1}{\nu_i} RA_i,$$

where I_i is the Raman intensity, RA_i is the Raman scattering activities, ν_i is the wavenumber of the normal modes and ν_0 denotes the wavenumber of the excitation laser [23].

RESULTS AND DISCUSSION

Tautomeric Analysis

All the possible tautomeric forms of 4M2PI were calculated which are optimized by B3LYP/6-311++G(d,p) level of theory. The possible two stable tautomeric forms are given in Fig. 3, which shows the possibility of proton transfer between the nitrogen atoms of imidazole ring. The total energies and the relative energies of the different tautomeric forms of

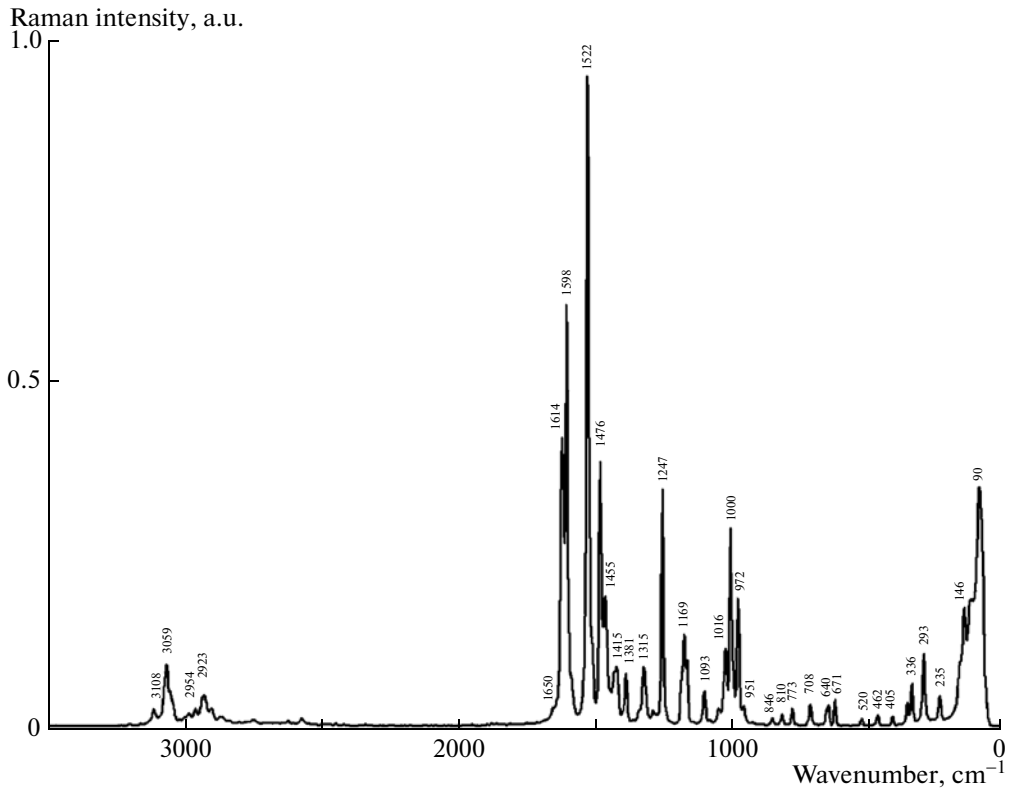

Fig. 2. Experimental FT-Raman spectra of 4-methyl-2-phenylimidazole molecule.

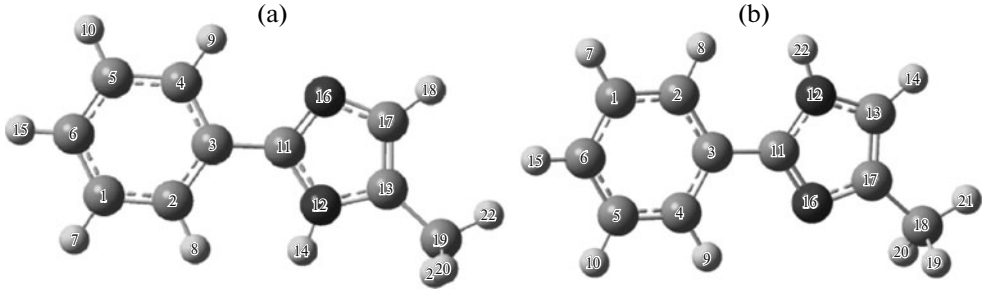

Fig. 3. All tautomeric forms and atomic numbering of 4-methyl-2-phenylimidazole (4M2PI). (a) Tautomer 1. Optimized energy—−496.73079735 a.u., Relative opt. energy—6.50 kJ/mol; (b) Tautomer 2. Optimized energy—−496.73153114 a.u., Relative opt. energy—0 kJ/mol.

4M2PI are presented in Fig. 3. Many attempts to investigate the tautomeric equilibrium structure of phenylimidazole molecule have been made using different calculation methods. It is determined that T_2 is more stable than T_1 by 3 kJ mol^{-1} for AMI and PM3 calculations by Ogretir and Yarligan [24]. Maye and Venanzi have calculated rotational barrier and energies of both T_2 and T_1 tautomeric forms of phenylimidazole [25]. They reported that the difference in energy is 7.5 kJ/mol^{-1} by T_2 compared with T_1. The tautomeric equilibrium structures of 4-phenylimidazole molecule were investigated by our previous paper [12] and is determined that T_2 is more stable than T_1 by 5.27 kJ/mol for B3LYP/6-311G(d,p) level of theory. In the present work, it is clear that the T_2 tautomer has the lowest energy and is the most stable form. The energy difference between T_1 and T_2 tautomer is 6.50 kJ/mol (at B3LYP/6-311G++(d,p) level of theory). This confirms that the 4M2PI is the only stable tautomer in gas phase. So, finally we taken T_2 tautomeric form was used in the future calculations such as vibrational and NMR spectra of the 4M2PI molecule.

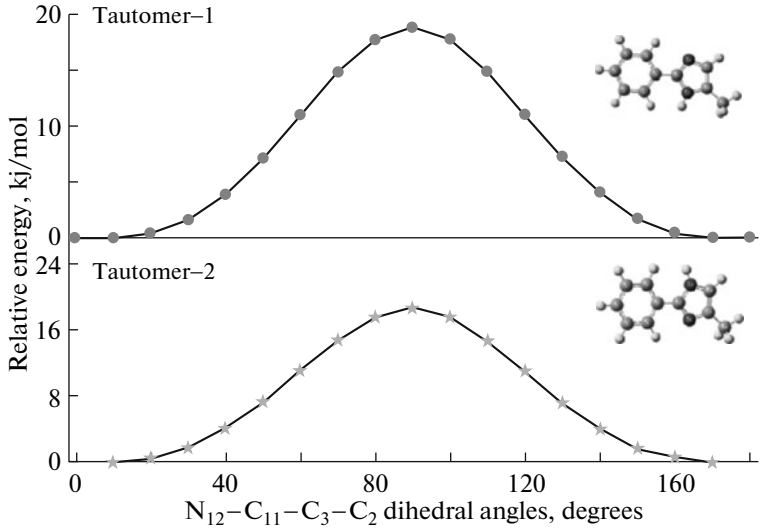

Fig. 4. Potential energy surface of all tautomeric forms of 4-methyl-2-phenylimidazole (4M2PI) for dihedral angle N_{16}–C_{11}–C_3–C_4.

Conformational Analysis

In order to reveal all possible conformations of 4M2PI, a detailed potential energy surface (PES) scan in N_{16}–C_{11}–C_3–C_4 dihedral angles was performed. The scan was carried out by minimizing the potential energy in all geometrical parameters by changing the torsion angle for every 10° for a 180° rotation around the bond. The shape of the potential energy as a function of the dihedral angle is illustrated in Fig. 4. It shows that T_1 tautomeric form was planar (N–C–C–C dihedral angle for 0°) and T_2 tautomeric form was twisted (N–C–C–C dihedral angle for 10°).

Optimized Structure

The optimized bond lengths and bond angles of the T_2 tautomeric form of the 4M2PI molecule at B3LYP/6-311-H-G(d,p) level is collected in Table 1. These optimized geometric parameters of 4-PI are compared with those of X-ray data [26].

VIBRATIONAL ANALYSIS

The 4M2PI molecule consists of 22 atoms. So, there are 60 vibrational modes. The 60 vibrational modes of 4M2PI have been assigned according to the detailed motion of the individual atoms. This molecule belongs to C_1 symmetry group. The experimental FT-IR and FT-Raman along with the calculated wavenumbers are given in Table 2. As seen in Table 2, IR and Raman intensities of 4M2PI are in consistency with the TED results. The experimental FT-IR and FT-Raman spectra are shown in Figs. 1–2.

Phenyl Group Vibrations

The aromatic C–H stretching vibrations are normally found between 3100 cm^{-1} and 3000 cm^{-1}. In this region the bands are not affected appreciably by the nature of substituents. The aromatic C–H stretching frequencies arise from the modes observed at 3062 cm^{-1} (a_{1g}), 3047 cm^{-1} (e_{2g}), 3060 cm^{-1} (b_{1u}) and 3080 cm^{-1} (e_{1u}) cm^{-1} of benzene and its derivatives [27]. In the present work, C–H stretching vibrations of 4M2PI molecule are observed at 3009 cm^{-1} (3011 cm^{-1} for FT-Raman spectra) and 3068 cm^{-1} (3059 cm^{-1} for FT-Raman spectra) in the FT-IR spectra. These peaks are predicted in the region 3011–3060 cm^{-1} for B3LYP/6-311++G(d,p) level of theory.

The aromatic C–H in-plane bending modes of benzene and its derivatives are observed in the region 1300–1000 cm^{-1}. Studies on the spectra of benzene shows that there are two degenerate e_{2g} (1178 cm^{-1}) and e_{1u} (1037 cm^{-1}) and two non-degenerate b_{2u} (1152 cm^{-1}) and a_{2g} (1340 cm^{-1}) vibrations involving the C–H in-plane bending [27]. In the case of 4M2PI the bands observed at 1139 cm^{-1}, 1165 cm^{-1}, and 1312 cm^{-1} in FT-IR and at 1158, 1169 cm^{-1}, and 1315 cm^{-1} in FT-Raman spectrum are assigned to the C–H in-plane bending vibrations. The C–H out of plane bending modes [28–31] usually medium intensity arises in the region 1000 cm^{-1}–600 cm^{-1}. The C–H out of plane bending results from b_{2g} (985 cm^{-1}), e_{2u} (970 cm^{-1}), e_{1g} (850 cm^{-1}) and a_{2u} (671 cm^{-1}) modes of benzene [27]. The aromatic C–H out of plane bending vibrations of 4M2PI are assigned to the medium to very strong bands observed at 829 cm^{-1} (816 cm^{-1} for DFT) and 968 cm^{-1} (972 cm^{-1} for DFT) in the infrared spectrum. These vibrations are observed at 671 cm^{-1}

Table 1. Optimized geometric parameters of 4M2PI

Bond Lengths (Å)			Bond Angles (°)			Dihedral Angles (°)		
Parameters	B3LYP	X-Ray*	Parameters	B3LYP	X-Ray*	Parameters	B3LYP	X-Ray*
$C_1–C_2$	1.392	1.388	$C_2–C_1–C_6$	120.2	121.0	$C_6–C_1–C_2–C_3$	−0.129	−0.720
$C_1–C_6$	1.393	1.367	$C_2–C_1–H_7$	119.6	120.3	$C_6–C_1–C_2–H_8$	179.5	171.8
$C_1–H_7$	1.084	1.017	$C_6–C_1–H_7$	120.1	115.5	$H_7–C_1–C_2–C_3$	−179.9	178.7
$C_2–C_3$	1.402	1.394	$C_1–C_2–C_3$	120.7	119.3	$H_7–C_1–C_2–H_8$	−0.336	7.630
$C_2–H_8$	1.085	1.017	$C_1–C_2–H_8$	118.5	121.0	$C_2–C_1–C_6–C_5$	−0.033	−0.040
$C_3–C_4$	1.403	1.385	$C_3–C_2–H_8$	120.7	118.3	$C_2–C_1–C_6–H_{15}$	−179.9	−167.0
$C_3–C_{11}$	1.465	1.470	$C_2–C_3–C_4$	118.5	118.4	$H_7–C_1–C_6–C_5$	179.8	−179.4
$C_4–C_5$	1.389	1.378	$C_2–C_3–C_{11}$	122.4	121.5	$H_7–C_1–C_6–H_{15}$	−0.123	13.54
$C_4–H_9$	1.082	1.017	$C_4–C_3–C_{11}$	119.0	120.0	$C_1–C_2–C_3–C_4$	0.216	1.380
$C_5–C_6$	1.395	1.388	$C_3–C_4–C_5$	120.5	121.3	$C_1–C_2–C_3–C_{11}$	−179.8	−176.5
$C_5–H_{10}$	1.084	1.017	$C_3–C_4–H_9$	118.4	120.5	$H_8–C_2–C_3–C_4$	−179.4	172.7
$C_6–H_{15}$	1.084	1.017	$C_5–C_4–H_9$	121.0	118.2	$H_8–C_2–C_3–C_{11}$	0.556	−5.220
$C_{11}–N_{12}$	1.370	1.370	$C_4–C_5–C_6$	120.4	119.9	$C_2–C_3–C_4–C_5$	−0.143	−1.340
$C_{11}–N_{16}$	1.322	1.336	$C_4–C_5–H_{10}$	119.5	115.1	$C_2–C_3–C_4–H_9$	179.8	179.8
$N_{12}–C_{13}$	1.380	1.384	$C_6–C_5–H_{10}$	119.9	121.8	$C_{11}–C_3–C_4–C_5$	179.8	176.5
$N_{12}–H_{22}$	1.006	1.069	$C_1–C_6–C_5$	119.4	119.3	$C_{11}–C_3–C_4–H_9$	−0.084	−2.280
$C_{13}–H_{14}$	1.077	1.017	$C_1–C_6–H_{15}$	120.2	118.2	$C_2–C_3–C_{11}–N_{12}$	3.716	40.40
$C_{13}–C_{17}$	1.374	1.373	$C_5–C_6–H_{15}$	120.3	120.0	$C_2–C_3–C_{11}–N_{16}$	−176.3	−143.6
$N_{16}–C_{17}$	1.374	1.306	$C_3–C_{11}–N_{12}$	124.3	127.9	$C_4–C_3–C_{11}–N_{12}$	−176.3	−137.4
$C_{17}–C_{18}$	1.494	–	$C_3–C_{11}–N_{16}$	125.4	122.9	$C_4–C_3–C_{11}–N_{16}$	3.583	38.40
$C_{18}–H_{19}$	1.093	–	$N_{12}–C_{11}–N_{16}$	110.1	114.1	$C_3–C_4–C_5–C_6$	−0.016	0.600
$C_{18}–H_{20}$	1.093	–	$C_{11}–N_{12}–C_{13}$	107.6	105.5	$C_3–C_4–C_5–H_{10}$	−179.9	−176.5
$C_{18}–H_{21}$	1.092	–	$C_{11}–N_{12}–H_{22}$	126.7	125.4	$H_9–C_4–C_5–C_6$	179.9	179.4
			$C_{13}–N_{12}–H_{22}$	125.6	123.7	$H_9–C_4–C_5–H_{10}$	0.012	2.310
			$N_{12}–C_{13}–H_{14}$	122.1	116.0	$C_4–C_5–C_6–C_1$	0.106	0.100
			$N_{12}–C_{13}–C_{17}$	105.6	105.7	$C_4–C_5–C_6–H_{15}$	−179.9	166.9
			$H_{14}–C_{13}–C_{17}$	132.1	128.7	$H_{10}–C_5–C_6–C_1$	−179.9	177.0
			$C_{11}–N_{16}–C_{17}$	106.8	104.4	$H_{10}–C_5–C_6–H_{15}$	−0.019	−16.150
			$C_{13}–C_{17}–N_{16}$	109.6	105.6	$C_3–C_{11}–N_{12}–C_{13}$	179.8	176.2
			$C_{13}–C_{17}–C_{18}$	128.7	–	$C_3–C_{11}–N_{12}–H_{22}$	1.002	−8.87
			$N_{16}–C_{17}–C_{18}$	121.6	–	$N_{16}–C_{11}–N_{12}–C_{13}$	−0.074	−0.13
			$C_{17}–C_{18}–H_{19}$	110.7	–	$N_{16}–C_{11}–N_{12}–H_{22}$	−178.9	174.7
			$C_{17}–C_{18}–H_{20}$	110.8	–	$C_3–C_{11}–N_{16}–C_{17}$	−179.8	−176.7
			$C_{17}–C_{18}–H_{21}$	111.1	–	$N_{12}–C_{11}–N_{16}–C_{17}$	0.037	−0.110
			$H_{19}–C_{18}–H_{20}$	107.3	–	$C_{11}–N_{12}–C_{13}–H_{14}$	−179.9	−175.6
			$H_{19}–C_{18}–H_{21}$	108.3	–	$C_{11}–N_{12}–C_{13}–C_{17}$	0.079	0.310
			$H_{20}–C_{18}–H_{21}$	108.3	–	$H_{22}–N_{12}–C_{13}–H_{14}$	−1.055	8.230
						$H_{22}–N_{12}–C_{13}–C_{17}$	178.9	175.8
						$N_{12}–C_{13}–C_{17}–N_{16}$	−0.059	−0.410
						$N_{12}–C_{13}–C_{17}–C_{18}$	179.8	–
						$H_{14}–C_{13}–C_{17}–N_{16}$	179.9	175.3
						$H_{14}–C_{13}–C_{17}–C_{18}$	−0.181	–
						$C_{11}–N_{16}–C_{17}–C_{13}$	0.014	0.220
						$C_{11}–N_{16}–C_{17}–C_{18}$	−179.8	–
						$C_{13}–C_{17}–C_{18}–H_{19}$	120.9	–
						$C_{13}–C_{17}–C_{18}–H_{20}$	−119.9	–
						$C_{13}–C_{17}–C_{18}–H_{21}$	0.498	–
						$N_{16}–C_{17}–C_{18}–H_{19}$	−59.13	–
						$N_{16}–C_{17}–C_{18}–H_{20}$	59.89	–
						$N_{16}–C_{17}–C_{18}–H_{21}$	−179.6	–

Table 2. Vibrational frequencies of 4-methyl 2-phenylimidazole

Mode No	Freq[a]	I^{b}_{IR}	I^{c}_{Raman}	Exp IR	Exp Raman	TED (%)[d]
ν_1	2	7.659	58.76			$T_{CCCN}(68) + T_{CCCC}(25)$ P–I
ν_2	90	0.231	2.500		90	$T_{CCCC}(22)$P + $T_{NCCH}(10)$P + $T_{NCCC}(14)$ P–I
ν_3	122	0.309	0.820		124	$T_{CCCH}(13) + T_{NCCH}(67)$ I–M
ν_4	125	4.679	1.746			$\delta_{CCC}(38)$ P + $\delta_{NCC}(45)$ I
ν_5	199	0.025	0.598			$T_{CCCC}(25) + T_{CCNC}(20)$ I–M
ν_6	284	1.088	5.162			$\delta_{CCC}(39) + \delta_{CCN}(24)$ I–M
ν_7	302	0.054	6.051		293	$T_{CNCC}(32) + T_{NCCC}(17)$ I
ν_8	338	0.806	1.425		336	$\delta_{CCC}(24)$P + $\delta_{NCC}(11)$ I
ν_9	392	1.340	0.049		405	$T_{CCCC}(63) + T_{CCCH}(35)$P
ν_{10}	458	8.251	1.477	440		$T_{CNCC}(10) + T_{CCNH}(21) + \gamma_{NCH}(11)$ P–I
ν_{11}	466	36.21	0.707	456	462	$\delta_{CCC}(25) + \gamma_{CCN}(35) + T_{CCNH}(11)$
ν_{12}	502	73.23	0.452	492		$T_{CCCC}(16) + T_{CCCH}(18)$P + $\gamma_{CNH}(13)$ I
ν_{13}	612	0.262	3.123	605		$\delta_{CCC}(57) + \delta_{CCH}(18)$ P
ν_{14}	618	18.75	0.444			$T_{NCCN}(19) + \gamma_{NCH}(23)$ I
ν_{15}	633	8.455	1.294	641	640	$\nu_{C-CH_3}(30)$I–M + $\delta_{CCC}(15)$ P
ν_{16}	677	95.56	0.028		671	$\gamma_{CCH}(84)$ P
ν_{17}	692	21.05	0.002	690		$\gamma_{CCH}(11)$ P + $T_{CCCN}(15) + T_{CNCN}(25)$ I
ν_{18}	692	6.891	2.697	709	708	$\nu_{C\text{-}CH3}(14)$ I–M + $\nu_{CC}(15)$ P–I + $\delta_{CCC}(15)$ P
ν_{19}	756	46.21	1.135	768	773	$\gamma_{NCH}(10) + T_{CCCH}(51)$ I
ν_{20}	813	45.00	0.161	812	810	$\gamma_{CCH}(48)$ P + $\gamma_{NCC}(23)$ I
ν_{21}	816	0.096	0.006	829		$\gamma_{CCH}(89)$ P
ν_{22}	889	5.030	0.012			$\gamma_{CCH}(79)$ P
ν_{23}	933	14.45	10.29	914	917	$\nu_{NC}(10) + \delta_{NCC}(11) + \delta_{CNC}(30) + \delta_{NCN}(14)$ I
ν_{24}	945	0.671	0.056		951	$\gamma_{CCH}(79)$ P
ν_{25}	963	3.673	9.715			$\nu_{NC}(14)$ I + $\delta_{CCH}(49)$ M
ν_{26}	972	0.523	0.117	968	972	$\gamma_{CCH}(90)$ P
ν_{27}	981	1.091	25.18			$\nu_{CC}(14) + \delta_{NCC}(11) + \delta_{CCH}(10)$ I
ν_{28}	1003	17.67	12.48		1000	$\nu_{CC}(11) + \nu_{CN}(15) + \delta_{CCC}(26)$ P–I
ν_{29}	1013	6.520	0.255	1022	1016	$\nu_{CC}(53) + \delta_{CCH}(24)$ P
ν_{30}	1025	1.018	0.060		1040	$\delta_{CCH}(66) + T_{NCCH}(13) + T_{CCCH}(15)$ M
ν_{31}	1053	4.434	0.284			$\nu_{CC}(15) + \delta_{CCH}(41)$ P + $\delta_{NCH}(10)$ I
ν_{32}	1068	18.05	2.487	1072	1075	$\nu_{NC}(30) + \delta_{NCH}(20) + \delta_{CCH}(13)$ I
ν_{33}	1143	0.250	2.324			$\delta_{CCH}(14)$ P + $\delta_{CNH}(11) + \nu_{CN}(31)$ I
ν_{34}	1149	7.722	26.12	1139	1158	$\nu_{CC}(15) + \delta_{CCH}(77)$ P
ν_{35}	1164	0.135	8.109	1165	1169	$\nu_{CC}(19) + \delta_{CCH}(74)$ P
ν_{36}	1197	54.48	26.57	1221		$\nu_{NC}(34) + \delta_{NCH}(19)$ I
ν_{37}	1253	6.176	5.898	1243	1247	$\nu_{NC}(51) + \nu_{CC}(16)$ I
ν_{38}	1277	2.772	0.910	1278	1284	$\nu_{CC}(61) + \delta_{CCH}(15)$ P
ν_{39}	1309	3.004	1.183	1312	1315	$\nu_{CC}(27) + \delta_{CCH}(59)$ P
ν_{40}	1345	13.39	0.648	1332	1336	$\nu_{CC}(14)$ P + $\nu_{NC}(33) + \delta_{CNH}(12)$ I
ν_{41}	1371	2.561	3.080			$\delta_{CCH}(13) + \delta_{HCH}(68)$ M
ν_{42}	1381	35.77	0.250		1381	$\nu_{NC}(44) + \delta_{CNH}(13)$ I + $\delta_{CCH}(14)$ P
ν_{43}	1430	24.61	59.71	1410	1415	$\delta_{CCH}(13) + \delta_{HCH}(58)$ M
ν_{44}	1433	13.53	1.827			$\nu_{CC}(20) + \delta_{CCH}(48)$ P

Table 2. (Contd.)

Mode No	Freq[a]	I^{b}_{IR}	I^{c}_{Raman}	Exp IR	Exp Raman	TED (%)[d]
ν_{45}	1441	34.48	27.48			$\delta_{HCH}(30) + \delta_{CCH}(22) + T_{CCCH}(11)$ M
ν_{46}	1459	9.422	20.93	1463	1455	$\delta_{CCH}(42) + \nu_{CC}(12)$P + $\nu_{NC}(13)$ I
ν_{47}	1494	52.51	100		1476	$\nu_{CC}(18)$ P–I + $\nu_{CC}(15) + \nu_{NC}(14)$ I
ν_{48}	1557	47.11	3.383	1517	1522	$\nu_{CC}(47) + \nu_{CN}(10)$ I
ν_{49}	1572	36.62	0.597	1578		$\nu_{CC}(52) + \delta_{CCH}(15)$ P
ν_{50}	1591	19.22	77.28	1594	1598	$\nu_{CC}(70) + \delta_{CCH}(11)$ P
ν_{51}	2877	100	11.55	2867	2860	ν_{CH_3} (100) M Symm.
ν_{52}	2917	33.16	3.547	2921	2923	ν_{CH_3} (100) M Asymm.
ν_{53}	2971	17.63	2.413		2977	ν_{CH_3} (100) M Asymm.
ν_{54}	3011	25.57	0.706	3009	3011	$\nu_{CH}(97)$ P
ν_{55}	3023	0.243	2.251			$\nu_{CH}(99)$ P
ν_{56}	3033	41.96	2.349			$\nu_{CH}(97)$P
ν_{57}	3046	31.44	6.307			$\nu_{CH}(99)$ P
ν_{58}	3060	4.929	2.422	3068	3059	$\nu_{CH}(99)$ P
ν_{59}	3088	22.06	3.244	3107	3108	$\nu_{CH}(99)$ IMI
ν_{60}	3488	58.90	0.785			$\nu_{NH}(99)$

[a] Obtained from the wave numbers calculated at B3LYP/6-311++G(d, p) using scaling factors 0.967 (for wave numbers under 1800 cm^{-1}) and 0.955 (for those over 1800 cm^{-1}).
[b] Relative absorption intensities normalized with highest peak absorption equal to 100.
[c] Relative Raman intensities calculated by Raint software and normalized to 100.
[d] Total energy distribution calculated B3LYP 6-311G(d, p) level, TED less than 10% are not shown.

(677 cm^{-1} for DFT), 951 cm^{-1} (945 cm^{-1} for DFT) and 972 cm^{-1} (972 cm^{-1} for DFT) in the FT-Raman spectra. These CH vibrations (Stretching, in-plane and out-of-plane bending) are in good agreement with literature values of benzene [27–31]. Theoretical results are also in good agreement with the experimental values.

Benzene has two degenerate CC stretching modes at 1596 cm^{-1} (e_{2g}) and 1485 cm^{-1} (e_{1u}). Similarly the frequency of two non-legenerate modes were observed at 1310 cm^{-1} (b_{2u}) and 995 cm^{-1} (a_{1g}) in benzene [27]. The frequency of degenerate pair in benzene is fairly insensitive to substitution. Similarly the frequency of e_{1u} vibrations pair is also not very sensitive to substitution, though heavy halogens diminish the frequency [32]. In the present work, CC stretching vibrations of phenyl group are observed at 1022 cm^{-1} (1016 cm^{-1} for FT-Raman and 1013 cm^{-1} for DFT calculation), 1278 cm^{-1} (1284 cm^{-1} for FT-Raman and 1277 cm^{-1} or DFT calculation), 1578 cm^{-1} (1572 cm^{-1} for DFT calculation) and 1594 cm^{-1} (1598 cm^{-1} for FT-Raman and 1591 cm^{-1} for DFT calculation) cm^{-1} in the FT-IR spectra.

Imidazole Group Vibrations

The heteroaromatic molecule containing an N–H group occur in the region 3500–3220 cm^{-1}. The position of absorption in this region depends upon the degree of hydrogen bonding, and hence upon the physical state of the sample or the polarity of the solvent [12]. In the present work, this is only one NH stretching modes of imidazole ring. But, this peak is not observed in the experimental spectra (FT-IR and FT-Raman). Imidazole C–H vibrations are distinctly observed in FT-Raman at 3108 cm^{-1} as strong bands and at 3107 cm^{-1} in FT-IR as weak bands as expected [33]. Theoretically predicted wavenumbers at 3088 cm^{-1} are assigned to C–H stretching vibrations. The TED corresponds to this vibration is a pure mode with contribution of 99%. According to Güllüoğlu et al. [12] the C–N stretching appears at 1395 cm^{-1} for 4-phenylimidazole. For 4M2PI molecule, the series of bands observed in FT-IR at 1463, 1410, 1332, 1243, 1221, and 1072 cm^{-1} and in FT-Raman at 1455, 1415, 1381, 1336, 1247, and 1075 cm^{-1} makes significant contributions to N–C stretching mode. In the imidazole ring C–C stretching is observed in FT-IR at 1517 cm^{-1} and in FT-Raman at 1522 cm^{-1}.

Methyl Group Vibrations

The methyl group vibrational modes of the studied compound are observed in typical ranges for these vibrations, e.g., CH stretching modes in the region 3000–2900 cm^{-1}, asymmetric bending δ_{as} (CH_3) modes 1500–1420 cm^{-1}, symmetric bending δ_s (CH_3) modes in the range 1370–1420 cm^{-1}, rocking modes 1040–990 cm^{-1}, stretching ν (C–CH_3) 1150–1208 cm^{-1} and 947–958 cm^{-1}, wagging ω (C–CH_3) at about 400 and 275–256 cm^{-1} and torsion *T* (CH_3) modes in the range 90–200 cm^{-1} [34]. The C–H stretching mode in CH_3 occurs at lower wavenumbers than those of the aromatic ring (3000–3100 cm^{-1}). For the methyl group, the asymmetric stretching vibration ν_{CH_3} are observed at 2921 cm^{-1} and the symmetric stretching ν_{CH_3} appears in the region 2867 cm^{-1} in the FT-IR spectra. The FT-Raman wavenumbers of modes corresponding to the asymmetric stretching vibration and the symmetric stretching vibrations are 2860, 2923, and 2977 cm^{-1}. These peaks are predicted at 2877 cm^{-1} (mode nos: 51), 2917 cm^{-1} (mode nos: 52) and 2971 cm^{-1} (mode nos: 53) for DFT calculations. 1410 cm^{-1} (mode nos: 43) (1415 cm^{-1} for FT-Raman spectra, 1430 cm^{-1} for DFT calculation) peak assigned to the symmetric bending vibrations of methyl group in the FT-IR spectra. CH_3 rocking vibration is observed at 1040 cm^{-1} (mode nos: 30) in the FT-Raman spectra. The ν (C–CH_3) stretching vibrations are normally observed in the regions of 1150–1208 cm^{-1} and 947–958 cm^{-1}. In the present work, one of two (ν(C–CH_3)) stretching modes assigned at 641 cm^{-1} in the FT-IR spectrum and 640 cm^{-1} at FT-Raman spectra and corresponds to 633 cm^{-1} for the DFT calculations. Other ν (C–CH_3) stretching vibration is observed at 709 cm^{-1} in the FT-IR spectrum and 708 cm^{-1} at FT-Raman spectra and corresponds to 692 cm^{-1} for the DFT calculations. 124 cm^{-1} peak is assigned to the torsion CH_3 mode in the FT-Raman spectra. None of the asymmetric bending and wagging ω (C–CH_3) modes was observed in the both FT-IR and FT-Raman spectrum. The results showed that experimental and theoretical data were in good agreement.

NMR ANALYSIS

^{13}C and NMR chemical shifts were calculated using the GIAO method [18] at the B3LYP/6-311++G(d,p) level. GIAO procedure is somewhat superior since it exhibits a faster convergence of the calculated properties upon extension of the basis set used. Taking into account the computational cost and the effectiveness of calculation, the GIAO method seems to be preferable from many aspects at the present state of this subject. On the other hand, the density functional methodologies offer an effective alternative to the conventional correlated methods, due to their significantly lower computational cost. The isotropic chemical shifts are frequently used as an aid in identification of relative ionic species. It is recognized that accurate predictions of molecular geometries are essential for reliable calculations of magnetic properties. The experimental and calculated values for ^{13}C and ^{1}H NMR arc shown in Table 3.

Table 3. The experimental and predicted ^{13}C and ^{1}H isotropic chemical shifts (with respect to TMS, all values in ppm) for 4M2PI

Atoms	Exp.	B3LYP	Atoms	Exp.	B3LYP
C_{11}	147.229	150.25	H_{22}	7.836	8.95
C_{17}	130.414	146.15	H_9	7.818	8.65
C_3	128.861	135.72	H_8	7.411	7.74
C_5	128.857	133.58	H_7	7.361	7.63
C_1	128.857	133.57	H_{10}	7.358	7.60
C_6	128.351	132.64	H_{15}	7.339	7.52
C_4	123.201	130.08	H_{14}	6.856	6.90
C_2	123.201	126.23	H_{20}	2.327	2.32
C_{13}	124.891	117.54	H_{19}	2.231	2.31
C_{18}		14.42	H_{21}	2.192	2.19

The studied molecule has five hydrogen atoms in the phenyl ring and two hydrogen atoms in the imidazole ring and three hydrogen atoms in the methyl group. One hydrogen atom attached to the nitrogen atom of imidazole group. Other hydrogen atom attached to the carbon atoms. The signals of the aromatic proton were observed at 2.192–7.836 ppm. The N atom (i.e.) more electronegative property polarizes the electron distribution in its bond to adjacent carbon atom and decreases the electron density of the molecule, therefore the H_{22} chemical shifts value seems to be slightly larger than those of phenyl and imidazole ring carbon atom.

The chemical shifts obtained and calculated for the hydrogen atoms of methyl groups are quite low. All values are ≤2.5 ppm due to the shielding effect [35]. It is also true from above literature data in our present study the methyl protons at C_{18} appears as a singlet with three proton integral at 2.327, 2.231 and 2.192 ppm.

In the present study, the signals for carbons were observed at 147–124 ppm. The carbon atoms C_{11} and C_{17} are highly electropositive atom, it appear at higher chemical shift (147.229 and 130.414 ppm) due to more positive charge. The result in Table 3 shows that the range ^{13}C NMR chemical shift of the typical organic molecule usually is >100 [36–38], the accuracy ensures reliable interpretation of spectroscopic parameters. The title molecule 4M2PI falls with the above literature data except with the methyl carbon atoms. In the present study, the signal predicted at

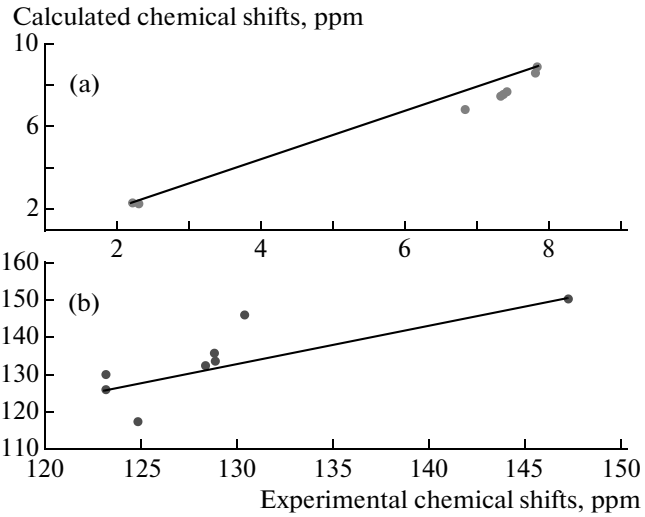

Fig. 5. The experimental and predicted ^{13}C and ^{1}H isotropic chemical shifts for 4M2PI.

14.42 ppm in ^{13}C NMR spectrum is assigned to C_{18} carbon atom. In ^{13}C NMR spectrum, in addition to the expected signals some additional signals are also observed. The additional signals (triplet at 77.33, 77.02, 76.70 ppm) are due to solvent peak.

The linear correlations between calculated and experimental data of ^{13}C NMR and ^{1}H NMR spectra are noted. Correlation coefficients of ^{13}C NMR and ^{1}H NMR are determined as 0.633 ppm and 0.984 ppm for 4M2PI. The data shows a good correlation between predicted and observed proton and carbon chemical shifts. The correlations of NMR spectra are presented in Fig. 5 for 4M2PI.

MOLECULAR ELECTROSTATIC POTENTIAL

Molecular electrostatic potential (MESP) mapping is very useful in the investigation of the molecular structure with its physiochemical property relationships [39–42]. Total electron density and molecular electrostatic potential of 4-methyl-2-phenylimidazole are shown in Fig. 6. The molecular electrostatic potential surface MESP which is a 3D plot of electrostatic potential mapped onto the iso-electron density surface simultaneously displays molecular shape, size and electrostatic potential values and has been plotted for 4M2PI using DFT method. The colour scheme for the MSEP surface is reflection rich or partially negative charge; blu-electron deficient or partially positive charge; light blu-slightly electron deficient region; yellow-slightly electron rich region, respectively. The MESP of 4M2PI shows clearly the electron rich centers of imidazole ring. The predominance of blue region in the total density surface corresponds to a net positive potential of 4M2P.

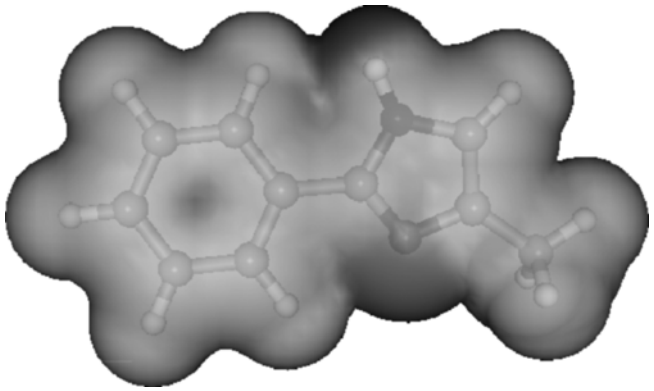

Fig. 6. Electrostatic potential map of 4-methyl-2-phenylimidazole molecule.

HOMO AND LUMO ANALYSIS

Highest occupied molecular orbital (HOMO) and lowest unoccupied molecular orbital (LUMO) are very important parameters for quantum chemistry. We can determine the way the molecule interacts with other species; hence, they are called the frontier orbitals. HOMO, which can be thought the outermost orbital containing electrons, tends to give these electrons such as an electron donor. On the other hand,

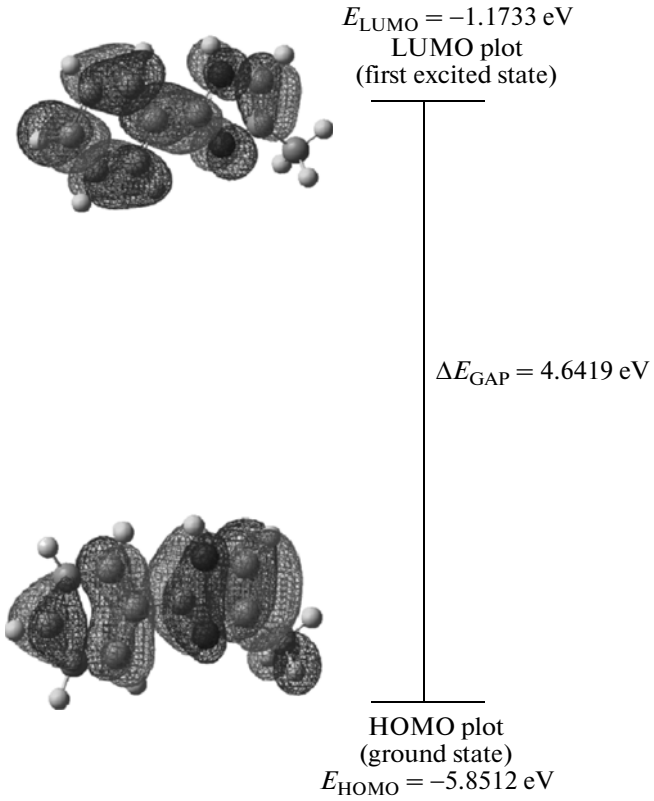

Fig. 7. The atomic orbital compositions of the frontier molecular orbitals of 4M2PI.

LUMO can be thought the inner most orbital containing free places to accept electrons [43]. Owing to the interaction between HOMO and LUMO orbital of a structure, transition state transition of $\pi-\pi^*$type is observed with regard to the molecular orbital theory [44]. Therefore, while the energy of the HOMO is directly related to the ionization potential, LUMO energy is directly related to the electron affinity. Energy difference between HOMO and LUMO orbital is called as energy gap that is an important stability for structures [45].

In addition, 3D plots of highest occupied molecular orbitals (HOMOs) and lowest unoccupied molecular orbitals (LUMOs) are shown in Fig. 7. According to B3LYP/6-311++G(d,p) calculation, the energy band gap (ΔE) (translation from HOMO to LUMO) of the molecule is about 4.6419 eV. The highest occupied molecular orbitals are localized mainly on all groups. On the other hand, the lowest unoccupied molecular orbitals are localized mainly on all groups without methyl group.

CONCLUSION

The optimized molecular structures, NMR spectra, vibrational frequencies and corresponding vibrational assignments of 4M2PI have been calculated using B3LYP/6-311++G(d,p) method. Comparison of the experimental and calculated spectra of the molecule showed that DFT-B3LYP method is in good agreement with experimental data. On the basis of agreement between the calculated and observed results, assignments of fundamental vibrational modes of 4M2PI were examined and some assignments were proposed. This study demonstrates that scaled DFT/B3LYP calculations are powerful approach for understanding the vibrational spectra of medium sized organic compounds. ^{1}H and ^{13}C NMR chemical shifts have been compared with experimental values.

ACKNOWLEDGMENTS

This work was supported by the Research Fund of Ahi Evran University Project Number: FBA-11-09.

REFERENCES

1. A. V. Chebanov, S. M. Desenko, and T. W. Gurley, *Azaheterocycles Basedon a,b-Unsaturated Carbonyls* (Springer, Berlin–Heidelberg, 2008).
2. Z. Jin, Natural Product Reports **26**, 382 (2009).
3. M. R. Grimmett, in *Comprehensive Heterocyclic Chemistry II*, Ed. by A. R. Katritzky, C. W. Rees, and E. F. W. Scriven (Pergamon, Oxford, 1996).
4. L. De Luca, Current Medicinal Chemistry **13**, 1 (2006).
5. I. S. Ahuja and I. Prasad, Inorg. Nucl. Chem. Lett. **12**, 777 (1976).
6. A. Donetti, E. Cereda, E. Bellora, A. Gallazzi, C. Bazzano, P. Vanoni, P. Del Soldato, R. Micheletti, F. Pagani, and A. Giachetti, J. Medicinal Chem. **27**, 380 (1984).
7. P. W. Erhardt, A. A. Hagedorn, and M. Sabio, Molecular Pharmacology **33**, 1 (1988).
8. D. J. Cram, P. Y. Sun, and L. S. Peng, J. Amer. Chem. Soc. **108**, 839 (1986).
9. D. J. Cram and H. E. Katz, J. Amer. Chem. Soc. **105**, 135 (1983).
10. V. T. D'Souza, K. Hanabusa, T. O'Leary, R. C. Gadwood, and M. L. Bender, Biochem. Biophys. Res. Commun. **129**, 727 (1985).
11. I. M. Mallick, V. T. D'Souza, M. Yamaguchi, J. Lee, P. Chalabi, R. C. Gadwood, and M. L. Bender, J. Amer. Chem. Soc. **106**, 7252 (1984).
12. M. T. Gulltioglu, Y. Erdogdu, J. Karpagam, N. Sundaraganesan, and S. Yurdakul, J. Mol. Struct. **990**, 14 (2011).
13. M. J. Frisch, G. W. Trucks, H. B. Schlegel, G. E. Scuseria, M. A. Robb, et al., *Gaussian 09, Revision A.02* (Gaussian, Inc., Wallingford CT, 2009).
14. G. Rauhut and P. Pulay, J. Phys. Chem. **99**, 3093 (1995).
15. Y. Erdogdu, O. Unsalan, and M. T. Güllüoğlu, J. Raman Spectrosc. **41**, 820 (2010).
16. Y. Erdogdu, O. Unsalan, M. Amalanathan, and Joe I. Hubert, J. Mol. Struct. **980**, 24 (2010).
17. Y. Erdogdu, O. Ünsalan, D. Sajan, and M. T. Güllüoğlu, Spectrochim. Acta Part A: Molecular and Biomolecular Spectroscopy **76**, 130 (2010).
18. R. Ditchfield, Molecular Orbital Theory of Magnetic Shielding and Magnetic Susceptibility **56**, 5688 (1972).
19. K. Wolinski, J. F. Hinton, and P. Pulay, J. Amer. Chem. Soc. **112**, 8251 (1990).
20. N. Azizi, A. A. Rostami, and A. Godarzian, J. Phys. Soc. Japan **74**, 1609 (2005).
21. M. Rohlfing, C. Leland, C. Allen, and R. Ditchfield, Chem. Phys. **87**, 9 (1984).
22. D. Michalska, Raint Program, Wroclaw University of Technology, 2003.
23. D. Michalska and R. Wysokinski, Chem. Phys. Lett. **403**, 211 (2005).
24. C. Ogretir and S. Yarligan, J. Molecular Struct. (THEOCHEM) **425**, 249 (1998).
25. P. V. Maye and C. A.Venanzi, Struct. Chem. **1**, 517 (1990).
26. R. M. Claramunt, M. D. S. Maria, L. Infantes, F. H. Cano, and J. Elguero, J. Chem. Soc., Perkin Transactions **2**, 564 (2002).
27. L. J. Bellamy, *The Infrared Spectra of Complex Molecules*, 3rd ed. (Wiley, New York, 1975).
28. H. Bohlig, M. Ackermann, F. Biiles, and M. Kudra, Spectrochim. Acta Part A: Molecular and Biomolecular Spectroscopy **55**, 2635 (1999).
29. E. Koglin, E. G. Witte, and R. J. Meier, Vibrational Spectrosc. **33**, 49 (2003).
30. A. A. El-Azhary, Spectrochim. Acta Part A: Molecular and Biomolecular Spectroscopy **55**, 2437 (1999).

31. Y. Wang, S. Saebao, and C. U. Pittman, Jr., J. Molecular Structure (Theochem) **281**, 91 (1993).

32. G. Varsanyi, *Assignments for Vibrational Spectra of Seven Hundred Benzene Derivatives* (Adam Hilger, London, 1974), Vol. I.

33. F. Billes, H. Endiedi, and G. Jalsovszky, J. Molecular Struct. (Theochem) **465**, 157 (1999).

34. M. Wandas, J. Lorenc, E. Kucharska, M. Maczka, and J. Hanuza, J. Raman Spectrosc. **39**, 832 (2008).

35. M. Karaback, M. Cinar, Z. Unal, and M. Kurt, J. Molecular Struct. **982**, 22 (2010).

36. H. O. Kalinowski, S. Berger, and S. Braun, *C-13NMR Spectroscopy* (Wiley, Chichester, 1988).

37. K. Pihlaja and E. Kleinpeter, *Carbon-13 Chemical Shifts in Structural and Stereo Chemical Analysis* (VCH Publishers, Deerfield Beach, 1994).

38. Y. Erdogdu, M.T. Gulluoglu, and M. Kurt, J. Raman Spectrosc. **40**, 1615 (2009).

39. I. Fleming, *Frontier Orbitals and Organic Chemical Reactions* (Wiley, New York, 1976).

40. J. S. Murray and K. Sen, *Molecular Electrostatic Potentials, Concepts and Applications* (Elsevier, Amsterdam, 1996).

41. J. M. Seminario, Recent Developments and Applications of Modern Density Functional Theory **4**, 800 (1999).

42. T. Yesilkaynak, G. Binzet, F. Mehmet Emen, U. Florke, N. Kulcu, and H. Arslan, Europ. J. Chem. **1**, 1 (2010).

43. G. Gece, Corrosíon Science **50**, 2981 (2008).

44. K. Fukui, *Theory of Orientation and Stereo Selection* (Springer-Verlag, Berlin, 1975).

45. D. F. V. Lewis, C. Ioannides, and D. V. Parke, Xenobiotica **24**, 401 (1994).